The Efficiency Characterization of the DSS-13 34-Meter Beam-Waveguide Antenna at Ka-Band (32.0 and 33.7 GHz) and X-Band (8.4 GHz)

D. D. Morabito
Communications Systems and Research Section

This article reports on the analysis of Ka-Band Antenna Performance Experiment (KaAP) antenna efficiency measurements acquired at the Goldstone DSS-13 research and development beam-waveguide (BWG) antenna between December 1993 and November 1995. The measurements were performed at the KaAP pedestal room feed position at 8.425 GHz (X-band) and 32.0/33.7 GHz (Ka-band). The measured antenna efficiency and ground station figure of merit (gain divided by operating system noise temperature) as a function of elevation angle and their uncertainties are discussed. Also described are the station and antenna configuration, the measurement technique, and the modeling used in the analysis processing. Also presented is the historical evolution of the Ka-band antenna efficiency measurements as progressive improvements and configuration changes to the DSS-13 BWG antenna and equipment were implemented.

I. Introduction

Several DSN telecommunications studies have shown that by utilizing Ka-band (31.8- to 32.3-GHz) frequencies over X-band (8.40 to 8.45 GHz) on a spacecraft-to-ground communications link, an advantage of 6 to 8 dB (a factor of 4 to 6 improvement) can be realized for a given spacecraft transponder weight, antenna size, and power allocation [1,2]. The link advantage can be used to increase data volume, decrease transmission time, decrease transmitter (XTMR) power on the spacecraft, decrease spacecraft antenna size, or allow for a smaller antenna on the ground. The increased advantage comes from increased antenna gain at the shorter wavelengths. However, the advantage can be reduced by higher atmospheric noise, antenna performance deficiencies, and weather susceptibility at Ka-band.

The concept of conducting a Ka-band link experiment to verify these studies and to discover any impediments that could deter this performance gain from being realized was proposed by Riley et al. in [3]. The first Ka-band link experiment at 33.7 GHz became reality with the Mars Observer project's Ka-Band Link Experiment (KaBLE) [4]. KaBLE utilized data acquired at DSS 13 from Mars Observer's Ka-band beacon and X-band signal between January and August of 1993.

With the loss of Mars Observer, it became important to continue the study of the link advantage until another spacecraft with Ka-band capability became available. The Ka-Band Antenna Performance Experiment (KaAP) was initiated at DSS 13 to evaluate antenna efficiency by observing natural radio sources at both Ka-band and X-band. These evaluations allow us to characterize the antenna efficiency at each frequency band as incremental performance improvements and configuration changes are realized. The ground station advantage of Ka-band relative to X-band is quantified using the acquired data from both bands. The effort also facilitates the demonstration and development of optimal operational strategies for beam-waveguide (BWG) antennas. The information gained will benefit the DSN and future flight projects considering Ka-band. The knowledge gained about the temporal variability of the Ka-band advantage due to weather effects will allow planners of future flight projects to develop robust, efficient telecommunication strategies at Ka-band.

Two spacecraft with Ka-band equipment will be available during the next two years. The Summer Undergraduate Research Fellowship satellite (SURFSAT-1), launched on November 4, 1995, is a DSN Technology Program flight experiment. SURFSAT-1 tracking data are currently being acquired for the purpose of characterizing this link advantage and will be presented in a future article. Mars Global Surveyor, scheduled for launch in November 1996, will carry KaBLE-II, another DSN Technology Program experiment. These missions allow Ka-band link advantage studies to continue using X-band and Ka-band spacecraft signal sources.

This article focuses on the antenna efficiency characterization of the DSS-13 BWG antenna using natural radio source observations. The DSS-13 research and development (R&D) BWG antenna and system used for the measurements are described in Section II. The data acquisition technique and model used in the analysis are described in Section III, and the results are presented and discussed in Section IV.

II. Ground Station and Equipment

A full discussion of the ground station and equipment was presented in a previous article focusing on the KaAP atmosphere noise temperature (tip-curve) measurement analysis [5]. This section focuses on details pertinent to the antenna efficiency analysis that were not fully discussed in [5] and on any upgrades. The locations of focal points and mirrors are displayed in Fig. 1.

A block diagram of the configuration for the KaAP system as realized for conducting these measurements is shown in Fig. 2. From a system level, the ground station can be broken into several subsystems: antenna, microwave, receiver (RCVR), data acquisition, monitor and control (M&C), and frequency and timing (FTS). Each subsystem will be described briefly below.

A. Antenna Subsystem

The pointing subsystem at Ka-band (17-mdeg half-power beamwidth (HPBW), which is defined as the full width between the half-power points of the antenna beam) requires more accurate pointing when tracking objects than it does at X-band (63-mdeg HPBW). Whereas an accuracy of 8 mdeg for X-band is sufficient, for Ka-band an accuracy of 2 mdeg is required to limit pointing loss to less than 0.5 dB. In the past, pointing calibrations had been shown to correct errors to about 5 mdeg rms in a blind or open-loop mode. Further reduction of pointing errors is realized using the AUTOBORE [6] automatic boresight technique, which corrects pointing over 5-min (typical) measurement periods. Typical pointing corrections from AUTOBORE are accurate to within 1- to-2 mdeg rms. Since pointing corrections are continually updated during successive observations of the same radio source, there is no systematic loss due to beam-pointing errors. Systematic losses due to subreflector focusing and BWG mirror misalignments may be present at some level, but these are not well quantified at this time.

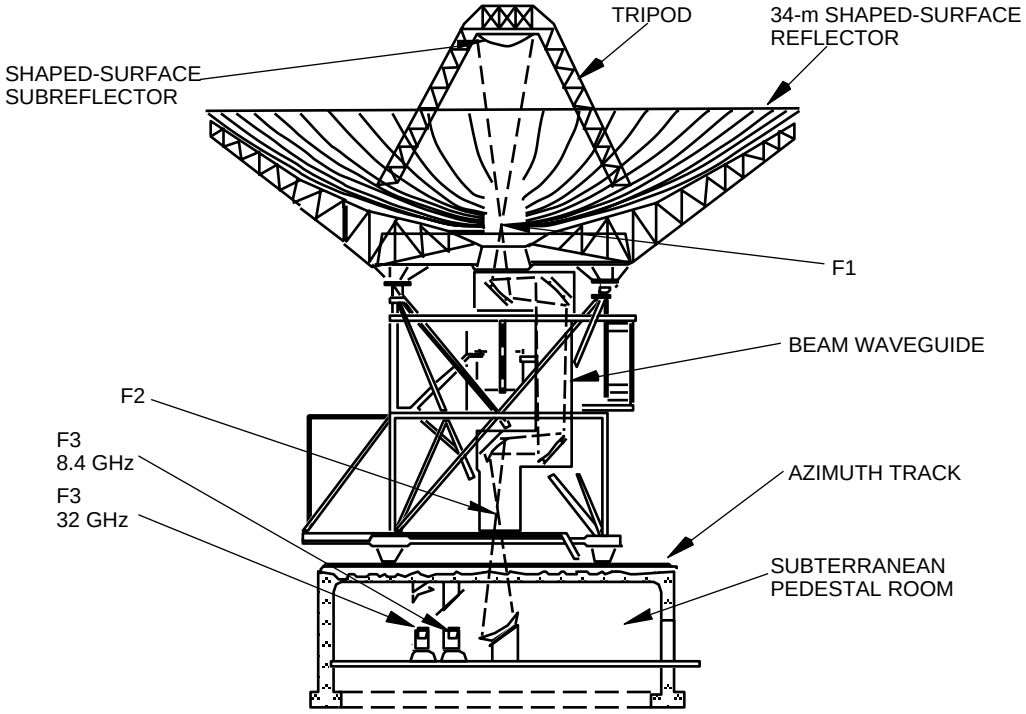

Fig. 1. Geometric configuration of reflectors and mirrors of DSS-13 BWG antenna along with positions of focal points.

B. Microwave Subsystem

The microwave subsystem takes advantage of the pedestal room layout to allow switching between different feed packages arranged in a ring around a rotating ellipsoid reflector. The feed package used for KaAP consists of an X-/Ka-band dichroic plate, a 25-dBi horn for X-band, a 26-dBi horn for Ka-band, and high-electron-mobility transistor (HEMT) low-noise amplifiers (LNAs) for both bands.

C. Receiver Subsystem

The receiver subsystem used for both frequency bands consists of RF-to-IF downconverters (DCs), an IF switch selector, fiber optics (FO) links from the pedestal room to the control room, and an IF distribution assembly in the control room.

The X-band downconversion is performed using an 8.1-GHz first local oscillator (LO). The bandwidth of the second IF filter is 500 MHz. For Ka-band, two configurations have been used. During the 33.7-GHz data acquisition period (from December 1993 to October 1994), the incoming 33.7-GHz signal was mixed with a 25.2-GHz first LO followed by a 8.2-GHz second LO. The bandwidth of the second IF filter was 100 MHz. For the 32.0-GHz data acquisition system installed in late 1994, the incoming 32.0-GHz signal was mixed with a 23.6-GHz first LO followed by an 8.1-GHz second LO. The bandwidth of the second IF filter was 500 MHz. All LOs are coherent with the station FTS.

The downconverter outputs are fed into a switch selector, where they are input to the fiber optic system. The X- and Ka-band IFs are converted to optical signals, transmitted over fiber-optic links to the control room, converted back to IF where they are input to an IF distribution assembly (amplifiers and power dividers), and distributed to the subsystems in the control room.

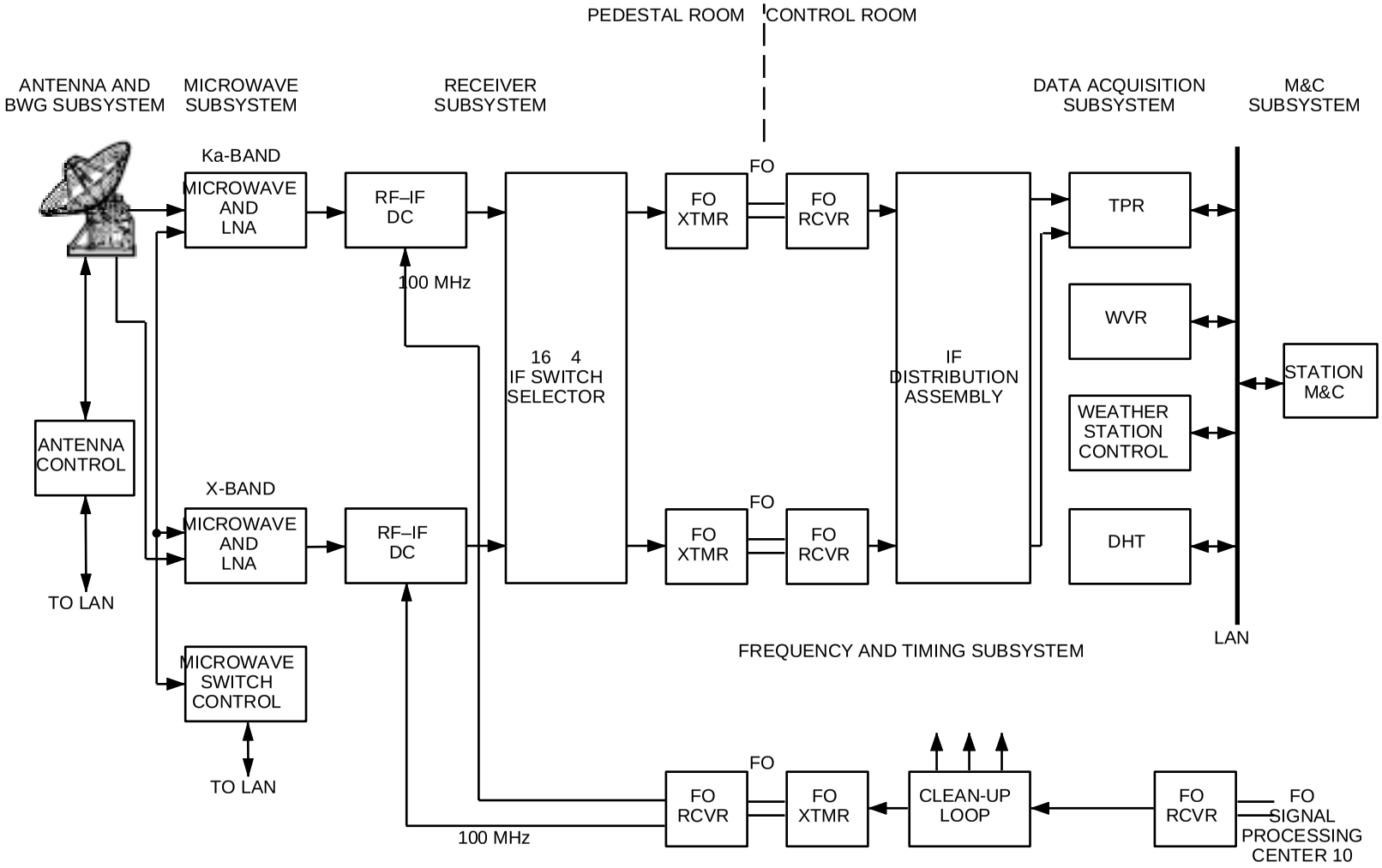

Fig. 2. The DSS-13 system used for KaAP X-/Ka-band.

D. Data Acquisition Subsystem

The instruments included in this subsystem include the total power radiometer (TPR) for measuring the operating system noise temperature (T_{op}), the water vapor radiometer (WVR) for measuring atmospheric noise, the weather station, and the data handling terminal (DHT) for displaying data from other instruments and recording KaAP-specific data to disk.

The TPR operates together with the microwave switch controller to perform calibrated T_{op} measurements during the track. The two incoming IF channels are filtered (20 MHz for X-band and 30 MHz for Ka-band) to limit the incoming noise bandwidth and any radio frequency interference (RFI). The bandwidth of these filters together with the radiometer integration time (5 s) define the contribution of the receiver noise, which lies below 0.01 K for both X-band and Ka- band systems. Variable step attenuators are used to set the power levels to a 1-μW level when the LNA input is on the ambient load with the noise diode on. Measurements of the total IF noise power are made with two Hewlett Packard (HP)8481 power sensors followed by HP437B or HP438A power meters—one each for X-band and Ka-band. The power sensors operate from 10 MHz to 18 GHz within 100-pW to 10-μW-level power values. A local computer platform reads these measurements and converts them to T_{op} values at a sampling rate of once per second, based on the transfer function derived from each calibration.

Calibrations are performed regularly throughout the track, alternating with the boresight observations. An initial set of calibrations at zenith is always performed at the beginning of a track (known as a PRECAL) and sometimes at the end of a track (known as a POSTCAL). During each calibration, the TPR measures the total IF noise power while the HEMT input is switched from sky, to sky plus noise diode, to ambient load, and to ambient load plus noise diode. The measurements are converted into a transfer function (T_{op} versus total noise power) and also allow for the correction of any nonlinearity that may be present. A detailed discussion of the system calibration methodology is provided in [7].

The R6 WVR [8] is a small stand-alone microwave radiometer package, positioned near the antenna, that measures the noise temperature contribution of water in the atmosphere in vapor and liquid form. In late 1995, the R6 WVR was replaced by the improved JTO3 WVR.

A "weather system" samples and records a range of meteorological parameters, including atmospheric pressure, air temperature, relative humidity, wind speed, and wind direction. The data are stored locally and routed through the M&C computer to the DHT, a central storage device.

E. Monitor and Control Subsystem

All of the subsystems are linked together into an operational system with a high degree of flexibility known as the monitor and control (M&C) subsystem. The main strength of the M&C is its user's interface, a window-driven display system configured by operators rather than developers. Early data were acquired on an M&C system that ran on a 486 PC platform. Another software package previously used for data acquisition, DEXTERITY, runs on a SUN workstation and is now the current backup.

In keeping with the goal to develop semiautomated monitor and control of operational procedures in the DSN, an operational prototype known as link monitor control operator assistant (LMCOA) was implemented at DSS 13 [9]. The LMCOA automation software was developed in a SUN/UNIX environment in C and RTworks. Originally targeted for automating KaBLE experiments, LMCOA was successfully implemented for KaAP.

Interfacing to the other subsystems is provided by the local area network (LAN). Each subsystem host computer taps into the LAN through a special board plugged into its chassis. A driver for handling real-time commands is loaded into the host computer's random access memory (RAM) at power-up.

F. Frequency and Timing Subsystem

KaAP benefits from fiber-optics technology in two areas. For frequency and timing, all of the sensitive reference frequency distributions are made with optical fiber. Distribution of the reference first LO to the downconverters in the pedestal room also makes use of fiber. The second use of fiber optics is the transmission of the broadband IF signals from the pedestal room to the control room, which has improved stability over that of coaxial cable.

III. Data Acquisition and Analysis

Since the KaAP data acquisition began in December 1993 after the end of the KaBLE experiment, the antenna efficiency measurements were acquired on a routine basis. Each time a configuration change was implemented, the performance determined from the new set of measurements was compared with that of the previous configuration. Any resulting change in antenna efficiency was compared with available predictions. The observation strategy, the model used to process the data, the observed radio sources, and the estimated uncertainties will be described here.

A. Description of the Measurement Sequence

KaAP uses dual-frequency observations of natural calibrator radio sources at Ka-band (33.7 and 32.0 GHz) and X-band (8.425 GHz), producing estimates of the antenna efficiency at each frequency. Each pass or experiment consists of a series of radio source observations distributed over different parts of the sky over a wide elevation angle range. There are typically one to two tracks per month, with each lasting from 8 to 24 hours in duration. Each track consists of a series of boresight observations of different radio sources, a series of radiometer calibrations that also are used to measure any small amount of system nonlinearity that may be present, and tipping curves used to estimate the effect of the atmosphere. The boresight observations alternate with the calibrations during the main body of the pass, with tipping curves usually performed at the start or end of the pass.

A sequence consisting of an X-band boresight, a Ka-band boresight, and radiometer calibrations at both X-band and Ka-band were normally performed for each measurement cycle of a source when the KaAP effort first started. In recent months, the tracks consisted primarily of Ka-band-only boresight observations, while the X-band T_{op} measurements were captured in TPR files intended for later processing.

1. Boresight Observations. Each boresight observation of a radio source involves stepping the antenna beam across the radio source while taking operating system noise temperature, T_{op}, measurements using the TPR. A peak noise temperature due to the source is estimated by fitting a linearized Gaussian beam model [6] over the T_{op} measurements in two orthogonal directions across the radio source: in cross-elevation (XEL) and in elevation (EL). The model is fit over the a priori on-source point (0 dB), the half-power down (-3 dB) points, and the off-source points. In cases where 7-point boresights are performed, the algorithm allows for acquisition of both X-band and Ka-band data. The solution yields the peak noise temperature due to the radio source, ΔT_{pk}; an estimate of the half-power beamwidth, θ_{HP}; and an estimate of the pointing correction relative to the accumulated pointing correction just prior to the boresight observation, $\Delta\theta$, in each direction.

The peak source noise temperatures are converted into estimates of antenna efficiency using the radio source's flux density and corrections for the angular flux distribution over the antenna beam, atmospheric attenuation (to refer the measurements to zero atmosphere), and any system nonlinearity that may be present.

2. System Calibrations. In addition to the boresight observations, radiometer calibrations are routinely conducted to correct for gain changes as the experiment progresses and to allow the system nonlinearity to be determined. The radiometer calibrations are described in Section II.D.

3. Tipping-Curve Measurements. In addition to the boresight observations and system calibrations, a sequence of tip-curve observations is routinely performed to characterize the atmosphere. These provide a means of determining the atmospheric loss factor used to refer the antenna efficiency measurements to zero atmosphere and the atmospheric noise temperature used for statistical cross-comparisons with independent WVR and surface-model estimates.

The tipping curves were usually done at the start or end of a track, with each lasting about 30 min. The tipping-curve acquisition consists of a set of cold-sky operating system noise temperature measurements at elevation angles that span from near the horizon to zenith. Normally, the atmosphere is sampled from 1 air mass (zenith) to about 4 air masses (14.5-deg elevation). These measurements were described in detail in a previous article [5].

B. Description of the Antenna Efficiency Model

Given a radio source of known flux density, the increase in operating system noise temperature as determined by the boresight measurements (peak source noise temperature fit over a linearized Gaussian model) is a measure of the antenna efficiency. The antenna efficiency measurement for the BWG antenna is referenced at the plane where the ambient load is inserted during calibrations. This measurement accounts for power losses of the main reflector, subreflector, BWG mirrors, dichroic plate, and any feed package loss, including waveguide (WG) up to the ambient load plane. For X-band, the antenna efficiency is referred to the input of the HEMT, where an ambient load is inserted by a waveguide switch during calibrations. For Ka-band, the antenna efficiency is referred to the input of the feedhorn, where an ambient load is swung over it during calibrations.

Given one received component of a randomly polarized radio source, the flux density is given by

$$S = \frac{2k\Delta T C_r C_p}{A_e} \tag{1}$$

where

$S =$ radio source flux density, W/(m^2-Hz)

$\Delta T =$ radio source noise temperature increase one would measure in a vacuum, K

$A_e =$ effective area of antenna, m^2

$C_r =$ source size correction

$C_p =$ pointing correction

$k =$ Boltzmann's constant, (1.38062×10^{-23} W/(K-Hz))

The source size correction, C_r, accounts for extended structure over the antenna beam and is equal to 1.0 for a point source. A standard unit for flux density, S, is the Jansky (Jy), where 1 Jy = 10^{-26} W/m^2-Hz. The pointing correction, C_p, is equal to 1.0 when there is no mispointing.

The AUTOBORE program performs sequential cross-elevation (XEL) and then elevation (EL) cuts of a radio source. The measured increases in operating system noise temperature due to a radio source are ΔT_{xel} and ΔT_{el} in the cross-elevation and elevation directions, respectively.

The best estimate of the source noise temperature increase, ΔT_m, is the average

$$\Delta T_m = \frac{\Delta T_{xel} + \Delta T_{el}}{2} \tag{2}$$

In order to estimate the antenna efficiency one would measure in a vacuum, the source noise temperature measurements, ΔT_m, are corrected by the atmospheric loss factor, $L_{atm}(\theta)$, where θ now denotes elevation angle. In the past, this loss factor was estimated using a weather model with surface meteorological measurements as input.[1] For this analysis, the data from the tipping curves conducted during each pass were used to determine $L_{atm}(\theta)$ (see [5]). Hence, ΔT is estimated from ΔT_m [Eq. (2)] using

$$\Delta T = L_{atm}(\theta) F_{lin} \Delta T_m \tag{3}$$

where F_{lin} is the system linearity factor determined from the radiometer calibration data. For Goldstone, typical zenith values of attenuation, $10 \log(L_{atm})$, as determined by the tip-curve measurements, are 0.035 dB at X-band and 0.15 dB at Ka-band.

Given that the effective area of the antenna is related to the antenna efficiency, ϵ, and antenna diameter, D, by

$$A_e = \frac{\epsilon \pi D^2}{4} \tag{4}$$

we can relate ϵ to the other parameters by combining Eqs. (1), (3), and (4) as follows:

$$\epsilon = \frac{8 k L_{atm}(\theta) F_{lin} \Delta T_m C_r C_p}{S \pi D^2} \tag{5}$$

Another measure of antenna performance is the figure of merit, G/T_{op}, or effective gain of the antenna, G, divided by the operating system noise temperature, T_{op}. Since G/T_{op} is used for spacecraft-to-ground link studies, the effects of the atmospheric loss (which was removed in the measured antenna efficiency ϵ) is included so that variations over a wide range of atmospheric conditions can be studied. The effective gain, G, is related to ϵ by

$$G = \frac{\epsilon}{L_{atm}} \left(\frac{\pi D}{\lambda} \right)^2 \tag{6}$$

where D is the antenna diameter, m, and λ is the observing wavelength, m. Therefore,

$$\frac{G}{T_{op}}(\theta) = \frac{\epsilon(\theta) \pi^2 D^2}{L_{atm}(\theta) T_{op}(\theta) \lambda^2} \tag{7}$$

T_{op} includes all contributions seen by the antenna (including cosmic, atmosphere, main structure and mirrors, feed package, amplifier, and follow-on). Typical zenith values of T_{op} for DSS 13 at the KaAP feed position are 40 K at 8.4 GHz and 55 K at 32 GHz. T_{op} is discussed in detail in [5].

[1] Such a model is SDSATM4S, S. Slobin, personal communication, Jet Propulsion Laboratory, Pasadena, California, February 8, 1993.

C. Radio Source Calibrators

The flux densities, uncertainties, and the source-size correction factors of the observed natural radio sources have been derived from independent studies and are listed in Table 1. The 8.4- and 32-GHz values for 3C274 and DR21 are from Richter,[2] and the values for the variable source 3C84 are nominal baseline values. The tabulated C_r's assume a 34-m antenna with HPBWs of 63 mdeg for 8.42 GHz and 16.8 mdeg for 32 GHz.

Table 1. Extragalactic radio sources used for efficiency calibration.

Source	Frequency, GHz	S, Jy	σ_s/S, percent	C_r	Reference
3C274	8.425	44.69	2.4	1.087	Footnote 2
	32.0	16.22	3.1	1.270	Footnote 2
	33.7	15.62	3.1	1.270	—[a]
DR 21	8.425	19.47	2.3	1.004	Footnote 2
	32.0	18.2	2.3	1.05	Footnote 2
3C84	8.425	24.0	—	1.0	Baseline
	32.0/33.7	15.1	—	1.0	Baseline

[a] P. Richter, personal communication, Jet Propulsion Laboratory, Pasadena, California, December 13, 1993.

The radio galaxy 3C274 is used as the principal calibrator at X-band and Ka-band and establishes the peak flux density near 45-deg elevation as well as curve shape over a wide elevation angle range. Since 3C274 is a low declination source, a higher declination source, 3C84, is used to supplement the measurements. Since 3C84 is a variable radio source, it is primarily used for elevation-angle curve shape information at the higher declination. The computed efficiencies for 3C84 (using the baseline flux density values of Table 1) are scaled such that its peak antenna efficiency matches that of the 3C274 data for each pass. The calibration source, DR21, had been observed for several early pre-1995 passes, but was dropped after it was found that a nearby confusion source was corrupting the data at Ka-band.

The determination of S and C_r for the planets Jupiter and Venus depend on additional parameters. The flux density, S, is related to the disk brightness temperature (see Table 2) at each observing wavelength, λ, as follows:

$$S = \frac{2kT_B\Omega}{\lambda^2} \tag{8}$$

where

$T_B =$ the blackbody disk temperature, K

$\Omega =$ the solid angle subtended by the planet, $\pi D_p^2/4\rho^2$

$D_p =$ the geometric mean of the planet diameter, km

$\rho =$ the distance to the planet, km

[2] P. Richter, *Radio Source List for Antenna Calibration*, DSN 890-269, JPL D-3801 (internal document), Jet Propulsion Laboratory, Pasadena, California, October 15, 1994.

Table 2. Brightness temperatures of the planets.

Planet	Frequency, GHz	T_B, K	σ_{T_B}/T_B, percent	Reference
Venus	8.4	652	2.3	[10]
	32.0	467	4	[10]
	33.7	461	4	[10]
Jupiter	8.4	210	4	[12]
	32.0	154	5	Text
	33.7	152	5	—[a]

[a] M. Gatti and M. Klein, personal communication, Jet Propulsion Laboratory, Pasadena, California, June 1994.

The source size correction factor for a planet, assuming uniform brightness and a Gaussian antenna beam, is given by[3]

$$C_r = \frac{\ln 2Q^2}{\left(1 - 2^{-Q^2}\right)} \tag{9}$$

where

$$Q = 2\frac{\sqrt{R_{eq}R_{pol}}}{\rho\theta_{HP}} \tag{10}$$

where θ_{HP} is the half-power beamwidth of the antenna in radians and R_{eq} and R_{pol} are the equatorial and polar radii of the planet, respectively. For Venus, $R_{eq} = R_{pol} = 6120$ km. For Jupiter, $R_{eq} = 71,492$ km and $R_{pol} = 66,854$ km.

The Ka-band brightness temperatures for Venus presented in Table 2 were extrapolated from a spectral curve given in [10]. For Jupiter, an appropriate blackbody correction was applied to the provided 152-K value at 33.7 GHz to get 154 K at 32.0 GHz. Because of larger measurement discrepancies relative to 3C274, the planets have not been routinely observed as calibration sources. Earlier data sets included observations of Venus and Jupiter, which are discussed in Section IV.

D. Antenna Efficiency Error Contributions

The uncertainty in the antenna efficiency measurements can be estimated using

$$\sigma_\epsilon(\theta) = \epsilon(\theta)\sqrt{\left(\frac{\sigma_s}{S}\right)^2 + \left(\frac{\sigma_{\Delta T_m}}{\Delta T_m}\right)^2 + \left(\frac{\sigma_{L_{atm}(\theta)}}{L_{atm}(\theta)}\right)^2 + \left(\frac{\sigma_{C_p}}{C_p}\right)^2} \tag{11}$$

where

[3] M. Klein, personal communication, Jet Propulsion Laboratory, Pasadena, California, February 3, 1994.

$\sigma_s/S =$ the uncertainty of the source flux density

$\sigma_{\Delta T_m}/T_m =$ the uncertainty of the source noise temperature measurement

$\sigma_{L_{atm}}/L_{atm} =$ the uncertainty of the atmospheric loss factor

$\sigma_{C_p}/C_p =$ the uncertainty due to any mispointing

The value of σ_s/S can be obtained from Table 1 for the extragalactic radio sources and inferred from σ_{T_B}/T_B in Table 2 for the planets. This contribution is assumed to be an absolute calibration error in the measurements.

The uncertainty $\sigma_{\Delta Tm}$ is an estimate of the source noise temperature measured by the radiometer during the measurement period. Typical uncertainties for 3C274 at Ka-band are about 0.1 K ($\Delta T_m \sim$ 2.3 K). The main contributors are expected to be gain instability and atmospheric noise during the AUTOBORE measurement period, while thermal noise is negligible. This term dominates the observed scatter of the measurements during a pass.

The atmospheric loss factor uncertainty, $\sigma_{L_{atm}}$, can be estimated from the expected variation of the atmospheric noise temperature over a pass. Because the tip curves are usually performed once per pass (not during the AUTOBORE measurements), L_{atm} is effectively a nominal estimate over the pass. Long-term variations in atmospheric attenuation over a pass thus define $\sigma_{L_{atm}}$, while short-term variations (within the period of the boresight measurement) would be manifested in $\sigma_{\Delta T_m}$.

Losses due to beam-pointing errors, σ_{C_p}, are expected to be small (<0.01 dB) since AUTOBORE is continually updating the pointing corrections. It is possible that errors due to mispointing may be as high as 0.5 percent, which is still below those attributed to radiometer and atmospheric noise. Systematic losses due to errors in subreflector focusing and beam-waveguide mirror misalignments will be reflected directly in the antenna efficiency measurements. Data acquired at other feed positions may have different peak efficiencies and elevation-dependent curve shapes because of such misalignments.

IV. Results

Figure 3 displays the measured efficiencies at X-band and Ka-band versus elevation angle for data acquired from February to November 1995 at the KaAP X-/Ka-band feed position. The X-band data will be discussed in Section IV.A, and the Ka-band data will be discussed in Section IV.B. Also discussed will be G/T_{op} performance (Section IV.C) and a history of DSS-13 Ka-band performance improvements (Section IV.D).

The antenna efficiency measurements, Eq. (5), gathered from different radio sources and different passes for a given frequency band and station configuration are combined into a common data set. An antenna efficiency versus elevation-angle curve is then least-squares fit to the data using a second-degree polynomial model:

$$\epsilon(\theta) = c_0 + c_1\theta + c_2\theta^2 \tag{12}$$

where the $c_i, i = 0, 1, 2$ are the solve-for coefficients and θ is the elevation angle of the observation. Table 3 lists the fitted coefficients of a second-degree polynomial fit over the X-band and Ka-band data [see Eq. (12)].

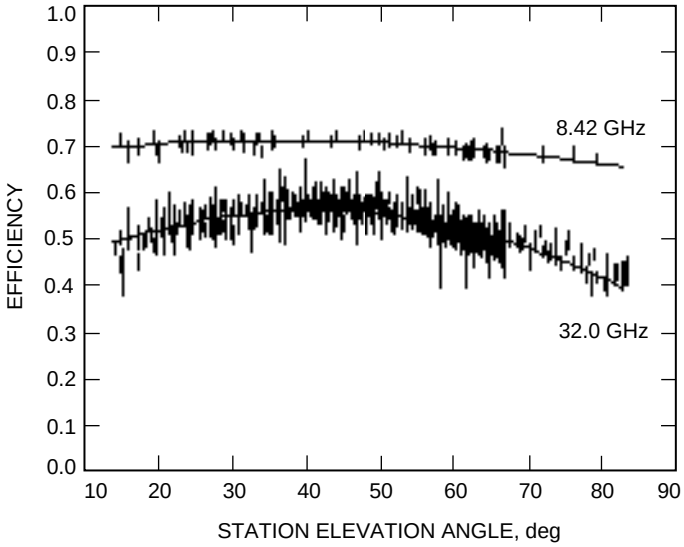

Fig. 3. Antenna efficiency versus elevation angle of the DSS-13 BWG antenna at X-band (8.4 GHz) and Ka-band (32.0 GHz), along with best-fit curves.

Table 3. Best-fit second-degree polynomial coefficients for DSS-13 X-band and Ka-band efficiencies (at F3, no atmosphere).

Frequency band	c_0	c_1	c_2	ϵ_{pk}, percent	θ_{pk}, deg	Source
X-band	0.675662	0.0019537	−0.000026679	71.1	36.6	All data
Ka-band	0.343756	0.0111280	−0.000136253	57.1	40.8	3C274
Ka-band	0.364831	0.0089171	−0.000100378	56.3	44.4	3C84
Ka-band	0.401467	0.0078074	−0.000094880	56.2	41.1	All data

A. Antenna Efficiency Measurements: X-band at F3

Provided in Fig. 3 are the data points with estimates of the error bars (excluding the absolute error contribution of the flux density) and the best-fit curve for X-band data acquired between February through May 1995. The rms error of the data points about the best-fit curve is 0.9 percent over 77 observations. The measured peak antenna efficiency is 71.1 percent at 37-deg elevation, which is in agreement with the 71.8-percent predicted value based on estimates of individual contributors (see Table 4).

A comparison of the measured KaAP X-band antenna efficiency with that of another X-band feed system at DSS 13 will now be presented. The X-band antenna efficiency of the S-/X-band feed system is 72.7 percent (without dichroic) [11]. The KaAP X-band antenna efficiency is 71.3 percent after removing the estimated effect of the dichroic plate. By next removing the estimated contributions of the individual feed packages, the efficiencies can be referred to the common antenna hardware. The resulting X-band efficiencies of 75.5 percent (S-/X-band feed position) and 75.9 percent (KaAP feed position) are in good agreement.

The X-band brightness temperatures of the planets Jupiter and Venus in Table 2 produced results (using earlier 1994 data) that were in reasonable agreement with those of 3C274. The peak X-band

Table 4. DSS-13 antenna efficiency accounting at the X-/Ka-band F3 feed position (estimated individual contributions, overall estimated and measured values).

Element	32.0 GHz[a]	33.7 GHz[b]	8.4 GHz[a]	Notes
Physical optics	0.8995	0.8650	0.8711	
Four upper BWG mirrors spillover	0.9888	0.9940	0.9940	
Two lower BWG mirrors spillover	0.9892	0.9965	0.9957	
Main reflector				
I^2R	0.9991	0.9991	0.99954	
Panel leakage	0.9975	0.9970	0.99992	
Gap leakage	0.9982	0.9982	0.9982	
rms surface	0.8532[c]	0.8378[c]	0.9889[c]	Assumes 0.31-mm rms normal surface error.
Subreflector				
I^2R	0.9991	0.9991	0.99954	
rms surface	0.9714	0.9683	0.9980	
Four BWG mirrors				
I^2R	0.9961	0.9961	0.99807	
rms surface	0.9437	0.9378	0.9960	
Two BWG mirrors				
I^2R	0.9982	0.9982	0.99903	
rms surface	0.9575	0.9530	0.9970	
BWG/Cassegrain VSWR[d]	0.9990	0.9990	0.999	
Waveguide				
I^2R	—[e]	—[e]	0.9480[f]	—[e,f]
VSWR	—[e]	—[e]	0.990	—[e]
Dichroic				
I^2R	0.9977[g]	0.9977[g]	0.9986	—[g]
VSWR	0.99[g]	0.99[g]	0.999	—[g]
Spillover	0.9983[g]	0.9719[g]	—	—[g]
Transmission rms	0.9778[h]	0.9778	—	—[h]
Feed support blockage	0.9180	0.9180	0.918	
Pointing squint	0.9954	0.9954	0.9954	
BWG alignments	0.99	0.99	0.9994	
Estimated (F3)	56.7%	52.1%	71.8%	—
Measured KaAP (F3)	57.1%[i]	52.2%[j]	71.1%[k]	—[i,j,k]

[a] All 32.0 and 8.4 GHz values are from [16] unless otherwise specified.

[b] All 33.7 GHz values are from W. Veruttipong, "Detailed Gain/Noise Budgets at X- and Ka-Bands for KABLE Experiment," JPL Interoffice Memorandum 3328-92-0190 (internal document), Jet Propulsion Laboratory, Pasadena, California, December 29, 1992, unless otherwise specified.

[c] D. Rochblatt, J. Withington, B. L. Seidel, and H. J. Jackson, op cit.

[d] Voltage standing wave ratio.

[e] Ka-band (33.7 and 32 GHz) estimated and measured efficiencies do not include waveguide losses as they are referred to the input plane of the horn.

[f] The X-band waveguide loss factor is from S. Stewart, personal communication, Jet Propulsion Laboratory, Pasadena, California, October 6, 1994.

[g] Ka-band dichroic values were inferred from [17] and [18].

[h] The value used is from W. Veruttipong, op cit.

[i] February to November 1995 32.0-GHz KaAP data (curve F of Fig. 7).

[j] September 1994 33.7-GHz KaAP data (curve D of Fig. 7).

[k] February to May 1995 8.45-GHz KaAP data.

antenna efficiency using Venus-only data was 2.1 percent lower than that of the 3C274-only data. Possible phase variations in Venus' brightness temperature, noted at other frequencies [13], may explain part of the 2.1-percent discrepancy, which is still consistent with the quoted overall 2.3-percent uncertainty given in Table 2. The peak X-band antenna efficiency using Jupiter-only data was within 0.1 percent of that using 3C274-only data.

B. Antenna Efficiency Measurements: Ka-band at F3

Figure 3 displays the antenna efficiency at 32.0 GHz (Ka-band) versus elevation angle in the form of the data points with estimated error bars (excluding the absolute error contribution in flux density) and the best-fit curve over the data acquired from February to November 1995. The rms of the data points about the best-fit curve is 1.9 percent over 444 total observations. The measured peak antenna efficiency of the 3C274-only data points (321 observations) is 57.1 percent at a 40.8-deg elevation, which is in reasonable agreement with the 56.7-percent predicted value based on independent estimates of individual contributors listed in Table 4. An estimate of the measured antenna efficiency for earlier data at the 33.7-GHz KaBLE frequency (52.2 percent) is also in agreement with its predicted value (52.1 percent) (Table 4).

Figure 4 displays the Ka-band data along with the 3C274 and the 3C84 best-fit curves. The northern-passing 3C84 high-elevation angle antenna-efficiency measurements (maximum elevation of 84 deg) lie above those of 3C274 (maximum elevation of 67.2 deg). For the KaAP feed position in the DSS-13 pedestal room (azimuth position of 174.5 deg), the antenna efficiency is higher for sources with declinations greater than 35 deg that rise and set in the north. The increased spread in the data between sources is attributed to a dependence in the antenna efficiency due to probable misalignments in the beam-waveguide mirrors. This behavior is similar to that noted by Alvarez et al. [14] for DSS 24's R&D Ka-band F3 feed position (azimuth position of 180 deg in the DSS-24 pedestal room).

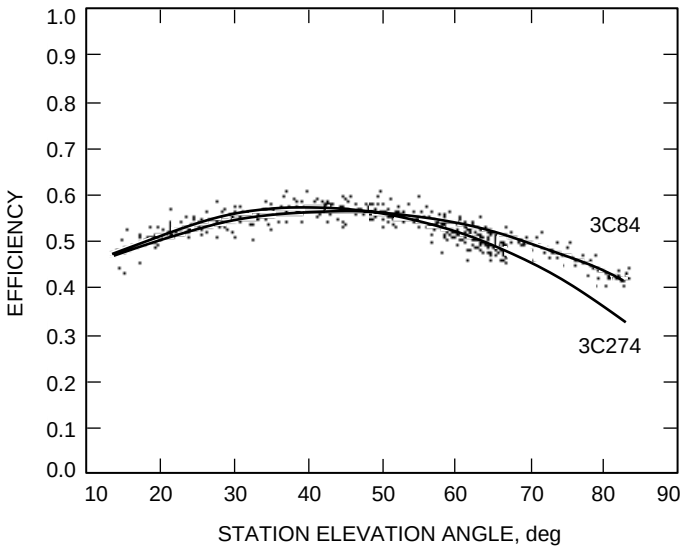

Fig. 4. Antenna efficiency versus elevation angle of the DSS-13 BWG antenna at Ka-band (32.0 GHz), along with best-fit curves for 3C274-only data and 3C84-only data.

The measured Ka-band efficiencies show no significant variation with azimuth after removing the elevation angle dependence from the data. This is consistent with the conclusion noted by others [11].

The sources used for the Ka-band antenna efficiency determination discussed above were the primary calibrator 3C274 and the variable source 3C84 (used primarily for curve shape). The planets Venus and Jupiter were observed for several passes performed during earlier 33.7-GHz sessions. The peak antenna

efficiency of the Venus data using $T_B = 461$ K in Table 2 was 7.3-percent below that of the 3C274 data. If the peak antenna efficiency using Venus data is scaled to match that of 3C274 data, the resulting $T_B = 430$ K still appears to be within the 1-σ uncertainty of the Steffes et al. emission spectrum [10]. Possible contributions to this discrepancy include errors in the relative flux calibration of Venus and 3C274, errors due to significant brightness temperature variation with phase angle [13], and possible modeling errors in estimating the source size correction of a planet. For the Jupiter data, using T_B given in Table 2, the estimated peak antenna efficiency was 1.5-percent below that using 3C274 data, which is within the 5 percent quoted uncertainty.

The gravity-induced roll-off of the antenna efficiency curve extrapolated to a 7.0-deg elevation angle (33.8-deg below the elevation angle of peak antenna efficiency) shows a projected degradation of about 1.4 dB (using 3C274 data). Holography performed at a 46.5-deg and a 12.7-deg elevation predicts a 2-dB degradation between these two points. The estimated 1.4-dB degradation of the KaAP curve is consistent with the 2-dB holographic prediction, as there is a large uncertainty in extrapolating the (3C274-only) KaAP curve to an elevation angle (7.0 deg) where there are no data. At a 20-deg elevation, the estimated 51.3-percent antenna efficiency corresponds to a degradation of 0.47 dB relative to the peak 57.1 percent value.

During certain passes, anomalous data points were observed when the measured wind speeds exceeded 32 km/h (20 mph) and the antenna was pointed directly into the direction of the oncoming wind or when the wind speed exceeded 48 km/h (30 mph). The majority of these data points were automatically removed due to AUTOBORE pointing offsets that exceeded a set 2-mdeg tolerance. Cases where the pointing errors were acceptable but the measured efficiencies were suspect occurred during periods of significant gain changes (noted upon inspection of the radiometer calibration data) and, thus, were deleted. A possible cause of the large gain variations is insufficient isolation of the pedestal room environment from outside weather changes. Data from passes that occurred during especially turbulent weather, such as rain, have also been removed from the data set due to the degradation in the boresight technique.

The rms scatter of the data about the fitted polynomials provides a measure of the noise in the data. For 3C274-only data, the rms scatter (1.6 percent) agrees well with that of 3C84-only data (1.7 percent). The major contributors to this scatter are expected to be radiometer gain instability, atmospheric noise variations, and error in determination of the atmospheric loss factors used to refer the measurements to zero atmosphere. Measured values of gain instability from radiometer calibration data are consistent with the 1.0-percent rms scatter of data acquired from a single source during a single pass, indicating that radiometer gain fluctuations are the dominant error source during these "good" weather passes.

The higher amount of scatter for the full data set combined over the several different passes, 1.6 percent, is likely due to differences in how accurately the L_{atm} corrections can be determined from one pass to another. The atmospheric loss factor is usually determined from a single tip-curve measurement, either at the start or end of a pass.

C. G/T_{op} Performance

The G/T_{op} figure of merit characterizes the ground station contribution used in link studies by spacecraft mission planners. Figure 5 is the G/T_{op} estimated from the data at both frequencies using Eq. (7). The relative link advantage of Ka-band over X-band plotted in Fig. 6 is the Ka-band G/T_{op} data point in Fig. 5 differenced from the fit value over the X-band data points at the observed Ka-band elevation angle. From Fig. 6, we see a 7- to 9-dB advantage of Ka-band relative to X-band for the current station configuration. However, if both Ka-band and X-band G/T_{op} measurements are adjusted for projected noise temperatures of improved future HEMT LNAs,[4] the resulting link advantage realistically lies between 6 to 8 dB.

[4] $T_{lna}(X) = 6$ K and $T_{lna}(K_a) = 13$ K, J. Shell, personal communication, Jet Propulsion Laboratory, Pasadena, California, June 12, 1995.

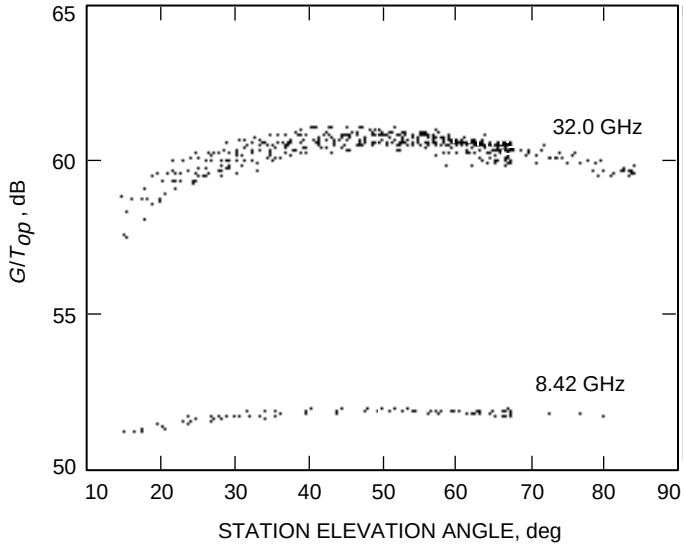

Fig. 5. The G/T_{op} figure of merit versus elevation angle of the DSS-13 BWG antenna at X-band (8.4 GHz) and Ka-band (32.0 GHz).

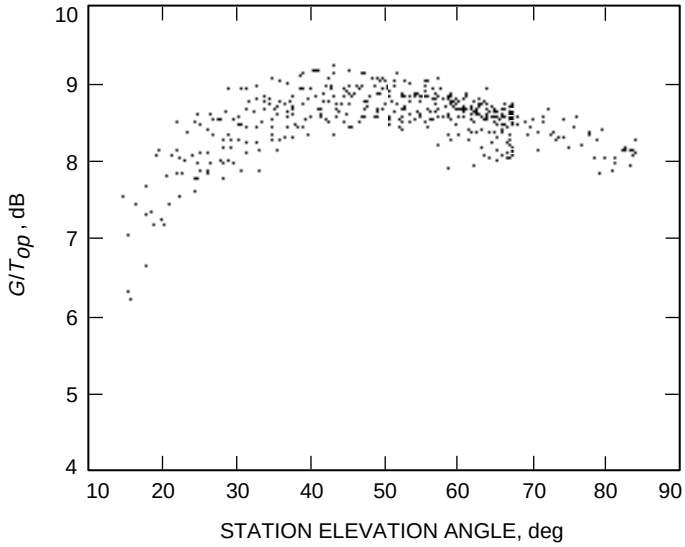

Fig. 6. The G/T_{op} ground station advantage (Ka-band over X-band) versus elevation angle of the DSS-13 BWG antenna.

D. History of DSS-13 BWG Performance Improvements at Ka-Band

Since the DSS-13 BWG antenna was first placed into operation in 1990, a series of performance improvements has been implemented. Figure 7 displays each curve that was fit from the measured Ka-band antenna efficiency data acquired between these configuration changes. Note the progressive improvement in peak antenna efficiency as each configuration change was implemented.

Curve A in Fig. 7 is the antenna efficiency curve measured in January 1991 during DSS 13's first configuration at 32 GHz as part of its postconstruction performance evaluation [15]. The data for this curve were acquired using a test package located at a different F3 feed position in the DSS-13 pedestal room.

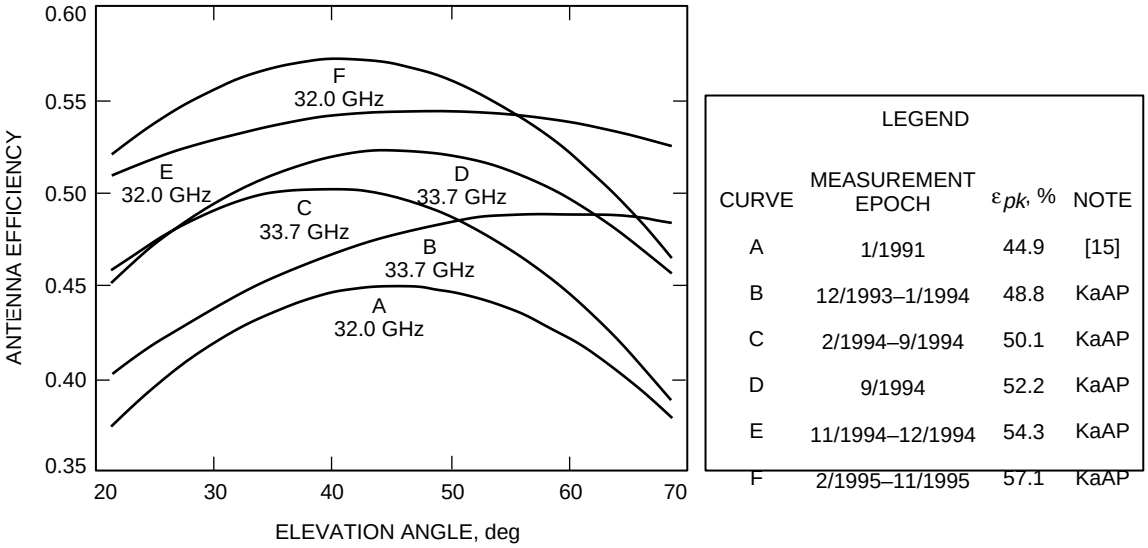

Fig. 7. A history of Ka-band performance measurements at DSS 13: Ka-band antenna efficiency versus elevation angle.

Initial theodolite and holography panel setting sessions were conducted in August and September 1990, resulting in 0.42-mm normal rms surface error of the main reflector.[5]

In January 1992, the panels were readjusted, with a resulting normal rms surface error of 0.38 mm corresponding to a predicted improvement of a factor of 1.060. Other activities that occurred during the interim between curves A and B were the stiffening of the turntable platform of the ellipsoid mirror in the pedestal room used to direct the incoming RF energy to the desired feed position and the removal of the bypass feed shroud.

The first KaAP sessions were conducted between December 1993 and January 1994 at the KaBLE frequency of 33.7 GHz. These data produced a peak measured antenna efficiency of 48.8 percent at a 59.5-deg elevation (curve B). The net improvement of the curve-B peak efficiency over that of curve A was found to be consistent with the expected improvement after taking into account all known configuration differences between the two sessions. However, as seen in Fig. 7, curve B is peaked significantly away from the 45-deg rigging angle at about 60 deg and may have been caused by the stiffening of the ellipsoid support structure with no follow-up mirror alignment activity.

The January through February 1994 holography session involved adjusting the panels in the outer two rings of the main reflector, resulting in an improved normal rms surface error of 0.31 mm, corresponding to a predicted improvement of 1.094 relative to session B or 1.142 relative to session A. A series of mirror alignment operations was also conducted to bring the peak of the antenna efficiency curve nearer 45 deg.[6] This next series of measurements (curve C) (February through September 1994) yielded a peak antenna efficiency of 50.1 percent at an elevation angle of 39.5 deg.

In September 1994, a manual adjustment of 5.1 mm (0.2 in.) in the subreflector lateral x-position was made. A small data set conducted shortly after showed a small improvement with a peak antenna efficiency of 52.2 percent at 45.4 deg (curve D of Fig. 7).

[5] D. Rochblatt, J. Withington, B. Seidel, and H. Jackson, "Performance Improvement of DSS 13 at the Rigging Angle by Unbending the Panels in Rings 8 and 9," JPL Interoffice Memorandum 3328-94-023 (internal document), Jet Propulsion Laboratory, Pasadena, California, March 23, 1994.

[6] R. Thomas, "DSS 13 Mirror Alignment," Planning Research Corporation Inc. Memorandum, Planning Research Corporation Inc., McLean, Virginia, February 18, 1994.

In October 1994, the KaAP Ka-band system was modified to receive the standard DSN-allocated frequency band at 32.0 GHz (replacing the KaBLE 33.7-GHz system). At the same time, additional subreflector x-position adjustments were made and a new subreflector look-up table was installed. The resulting November through December 1994 data set at 32.0 GHz showed an improved peak antenna efficiency of 54.3 percent at a 48.4-deg elevation angle, but with a significantly flattened curve (curve E of Fig. 7). The expected improvement in peak antenna efficiency at 32.0 GHz should have been significantly greater (with the same curve shape). It was found that the subreflector optimization procedures using low-resolution holography had been performed at another feed position in the pedestal room at DSS 13. Upon checking the ellipsoid and subreflector at the KaAP position using radiometry, it was found that a significant additional 1.3-mm (0.05-in.) subreflector z-position correction was required to increase the peak antenna efficiency.[7] The most recent data set (curve F in Fig. 7), discussed in Section IV.B, displays the improvement over curve E after applying this correction. The peak antenna efficiency of 57.1 percent occurs at a 40.8-deg elevation angle. The measured improvement of 0.2 dB is consistent with the 0.14-dB improvement predicted from holography.[8] This correction to the subreflector focusing has been applied for each KaAP pass conducted since then.

V. Conclusion

The KaAP antenna efficiency measurements acquired at the DSS-13 R&D BWG antenna between December 1993 and November 1995 have been presented. This effort will continue in order to characterize the antenna efficiency performance and Ka-band-over-X-band link advantage and to supplement measurements expected from spacecraft such as SURFSAT-1 and Mars Global Surveyor KaBLE-II.

Future improvements to the KaAP system and data analysis algorithms may include (1) incorporating the use of WVR data to calibrate the atmospheric loss factor in the antenna efficiency estimates, (2) simultaneous observations of the WVR and DSS-13 BWG antenna to allow more accurate estimates of the atmospheric loss factors, (3) the possible use of low-resolution holography at the KaAP feed position to obtain an independent prediction of the gravity deformation and to optimize the subreflector at the KaAP feed position (some logistic concerns need to be addressed); (4) raster scanning to obtain an improved fit of the peak source noise temperatures, offset angles, and HPBWs, (5) investigating improved brightness temperature models for the planets, including taking into account the phase angle dependence of Venus at Ka-band, (6) exploring the possibility of deriving an optimum setting of the M1 mirror to minimize any misalignments in the BWG system, (7) the employment of low-loss plastic wind covers over the beam waveguide openings to further isolate the pedestal room from outside temperature variations and wind susceptibility, (8) the use of the CAMMATIC structure deformation compensation system to improve gain at the lower elevation angles, and (9) the readjustment of the BWG mirrors.

Acknowledgments

I would like to thank R. Clauss, C. Stelzried, C. Edwards, D. Rochblatt, D. Bathker, M. Klein, and P. Richter for many informative discussions and comments; S. Slobin for his thorough review of the article; the DSS-13 station personnel for conducting the experiments and acquiring the data (G. Bury, C. Goodson, L. Smith, G. Farner, R. Reese, R. Littlefair, J. Crook, and J. Garnica); the operations support of L. Skjerve and L. Tanida for overseeing the KaAP experiments at

[7] V. Vilnrotter, personal communication, Jet Propulsion Laboratory, Pasadena, California, January 1995.

[8] D. Rochblatt, personal communication, Jet Propulsion Laboratory, Pasadena, California, March 17, 1995.

the station; E. Paulsen, M. Britcliffe, J. Bowen, V. Vilnrotter, and S. Stewart for providing information on equipment and station specifications; and T. Rebold for assistance in software development.

References

[1] J. G. Smith, "Ka-Band (32-GHz) Downlink Capability for Deep Space Communications," *The Telecommunications and Data Acquisition Progress Report 42-88, October–December 1986*, Jet Propulsion Laboratory, Pasadena, California, pp. 96–103, February 15, 1987.

[2] J. W. Layland and J. G. Smith, "A Growth Path for Deep Space Communications," *The Telecommunications and Data Acquisition Progress Report 42-88, October–December 1986*, Jet Propulsion Laboratory, Pasadena, California, pp. 120–125, February 15, 1987.

[3] A. L. Riley, D. M. Hanson, A. Mileant, and R. W. Hartop, "A Ka-Band Beacon Link Experiment (KABLE) with Mars Observer," *The Telecommunications and Data Acquisition Progress Report 42-88, October–December 1986*, Jet Propulsion Laboratory, Pasadena, California, pp. 141–147, February 15, 1987.

[4] T. A. Rebold, A. Kwok, G. E. Wood, and S. Butman, "The Mars Observer Ka-Band Link Experiment," *The Telecommunications and Data Acquisition Progress Report 42-117, January–March 1994*, Jet Propulsion Laboratory, Pasadena, California, pp. 250–282, May 15, 1994.

[5] D. D. Morabito and L. Skjerve, "Analysis of Tipping-Curve Measurements Performed at the DSS-13 Beam-Waveguide Antenna at 32.0 and 8.45 Gigahertz," *The Telecommunications and Data Acquisition Progress Report 42-122, April–June 1995*, Jet Propulsion Laboratory, Pasadena, California, pp. 151–174, August 15, 1995.
http://tda.jpl.nasa.gov/tda/progress_report/42-122/122C.pdf

[6] L. S. Alvarez, "Analysis and Applications of a General Boresight Algorithm for the DSS-13 Beam Waveguide Antenna," *The Telecommunications and Data Acquisition Progress Report 42-111, July–September 1992*, Jet Propulsion Laboratory, Pasadena, California, pp. 48–61, November 15, 1992.

[7] C. T. Stelzried and M. J. Klein, "Precision DSN Radiometer Systems: Impact on Microwave Calibrations," *Proc. of the IEEE*, vol. 82, pp. 776–787, May 1994.

[8] S. J. Keihm, "Water Vapor Radiometer Measurements of the Tropospheric Delay Fluctuations at Goldstone Over a Full Year," *The Telecommunications and Data Acquisition Progress Report 42-122, April–June 1995*, Jet Propulsion Laboratory, Pasadena, California, pp. 1–11, August 15, 1995.
http://tda.jpl.nasa.gov/tda/progress_report/42-122/122J.pdf

[9] L. F. Lee and L. P. Cooper, "Link Monitor and Control Operator Assistant: A Prototype Demonstrating Semiautomated Monitor and Control," *The Telecommunications and Data Acquisition Progress Report 42-115, July–September 1993*, Jet Propulsion Laboratory, Pasadena, California, pp. 124–134, November, 15, 1993.

[10] P. G. Steffes, M. J. Klein, and J. M. Jenkins, "Observations of Microwave Emission of Venus from 1.3 to 3.6 cm," *Icarus 84*, pp. 83–92, 1990.

[11] W. A. Imbriale, M. S. Esquivel, and F. Manshadi, "Novel Solutions to Low-Frequency Problems With Geometrically Designed Beam-Waveguide Systems," *The Telecommunications and Data Acquisition Progress Report 42-122, April–June 1995*, Jet Propulsion Laboratory, Pasadena, California, pp. 138–150, August 15, 1995.
http://tda.jpl.nasa.gov/tda/progress_report/42-122/122H.pdf

[12] I. de Pater and S. T. Massie, "Models of the Millimeter–Centimeter Spectra of the Giant Planets," *Icarus 62*, pp. 143–171, 1985.

[13] L. del Ciampo, *Centimeter Emission Variation of Venus*, Masters Dissertation in Space Science/Radioastronomy and Solar Physics, Instituto de Pesquisas Espaciais, São José dos Campos, Brazil, October 1989.

[14] L. S. Alvarez, M. J. Britcliffe, M. M. Franco, S. R. Stewart, and H. J. Jackson, "The Efficiency Calibration of the DSS-24 34-Meter Diameter Beam-Waveguide Antenna," *The Telecommunications and Data Acquisition Progress Report 42-120, October–December 1994*, Jet Propulsion Laboratory, Pasadena, California, pp. 174-187, February 15, 1995.
http://tda.jpl.nasa.gov/tda/progress_report/42-120/120A.pdf

[15] S. D. Slobin, T. Y. Otoshi, M. J. Britcliffe, L. S. Alvarez, S. R. Stewart, and M. M. Franco, "Efficiency Measurement Techniques for Calibration of a Prototype 34-Meter-Diameter Beam-Waveguide Antenna at 8.45 and 32 GHz," *IEEE Trans. on Microwave Theory and Techniques*, vol. 40, no. 6, pp. 1301–1308, June 1992.

[16] D. A. Bathker, W. Veruttipong, T. Y. Otoshi, and P. W. Cramer, "Beam-Waveguide Antenna Performance Predictions With Comparisons to Experimental Results," *IEEE Trans. on Microwave Theory and Techniques*, vol. 40, no. 6, pp. 1274–1285, June 1992.

[17] J. C. Chen, P. H. Stanton, and H. F. Reilly, "Performance of the X-/Ka-/KABLE-Band Dichroic Plate in the DSS-13 Beam Waveguide Antenna," *The Telecommunications and Data Acquisition Progress Report 42-115, July–September 1993*, Jet Propulsion Laboratory, Pasadena, California, pp. 54–64, November 15, 1993.

[18] J. C. Chen, "Computation of Reflected and Transmitted Horn Radiation Patterns for a Dichroic Plate," *The Telecommunications and Data Acquisition Progress Report 42-119, July–September 1994*, Jet Propulsion Laboratory, Pasadena, California, pp. 236–254, November 15, 1994.
http://tda.jpl.nasa.gov/tda/progress_report/42-119/119N.pdf